



A Journal of the Gesellschaft Deutscher Chemiker

# Angewandte Chemie

GDCh

International Edition

www.angewandte.org

## Accepted Article

**Title:** Peapod-like CoP@C nanostructure from phosphorization in low-temperature molten salt for high-performance lithium ion batteries

**Authors:** Zhiliang Liu, Sungjin Yang, Bingxue Sun, Xinghua Chang, Jie Zheng, and Xingguo Li

This manuscript has been accepted after peer review and appears as an Accepted Article online prior to editing, proofing, and formal publication of the final Version of Record (VoR). This work is currently citable by using the Digital Object Identifier (DOI) given below. The VoR will be published online in Early View as soon as possible and may be different to this Accepted Article as a result of editing. Readers should obtain the VoR from the journal website shown below when it is published to ensure accuracy of information. The authors are responsible for the content of this Accepted Article.

**To be cited as:** *Angew. Chem. Int. Ed.* 10.1002/anie.201805468  
*Angew. Chem.* 10.1002/ange.201805468

**Link to VoR:** <http://dx.doi.org/10.1002/anie.201805468>  
<http://dx.doi.org/10.1002/ange.201805468>

# Peapod-like CoP@C nanostructure from phosphorization in low-temperature molten salt for high-performance lithium ion batteries

Zhiliang Liu<sup>+</sup>, Sungjin Yang<sup>+</sup>, Bingxue Sun, Xinghua Chang, Jie Zheng<sup>\*</sup>, Xingguo Li<sup>\*</sup>

**Abstract:** A mild phosphorization process in low-temperature molten salt (NaCl-KCl-AlCl<sub>3</sub>) is developed to synthesize peapod-like CoP@C nanostructures by using low-toxic industrial PCl<sub>3</sub> as the phosphorus source and Mg as the reductant at 250 °C. Importantly, high using efficiency of the phosphorous source is achieved since only stoichiometric PCl<sub>3</sub> is required to complete the reaction. The molten NaCl-KCl-AlCl<sub>3</sub> not only provide a liquid environment but also participate in the electron transport by the reversible conversion of Al<sup>3+</sup>/Al redox couple. The obtained 0D-in-1D peapod CoP@C structure exhibits excellent lithium storage performance, delivering a superiorly stable capacity of 500 mAh g<sup>-1</sup> after 800 cycles at high current of 1.0 A g<sup>-1</sup>.

Transition metal phosphides (TMPs, MP<sub>x</sub>, M = Fe, Co, Ni, etc.) have intriguing applications in energy conversion and storage, such as electrocatalysis, photocatalysis, supercapacities, lithium-ion and sodium-ion batteries, thus attracting a great deal of attention in recent years.<sup>[1]</sup> For example, CoP is a promising anode material because of its high theoretical capacity (894 mAh g<sup>-1</sup>).<sup>[2]</sup> Synthesis of TMPs nanostructures is more difficult compared to metal oxides or sulfides. The main challenge is the phosphorization process. P vapor can be used for TMP preparation but usually requires very high temperature (> 500 °C) due to the inertness of the P<sub>4</sub> molecule in the gas phase.<sup>[3]</sup> Low temperature phosphorization requires P precursor with higher reactivity such as PH<sub>3</sub>.<sup>[4]</sup> To avoid using the highly toxic PH<sub>3</sub>, NaH<sub>2</sub>PO<sub>2</sub> is used as an alternative precursor, which yields PH<sub>3</sub> upon thermal decomposition.<sup>[1a, 1c, 2]</sup> Currently, NaH<sub>2</sub>PO<sub>2</sub> is the most commonly used precursor for TMPs preparation, which can convert metal or metal oxide precursors into TMPs at temperature around 350 °C and largely retain the nanostructure of precursors.<sup>[5]</sup> The above methods are based on the phosphorization in the gas phase. A clear drawback is that the highly toxic phosphorous precursors have to be used in large excess to ensure complete conversion to the phosphide phase.

In this work, we address the above challenge by phosphorization in low-temperature molten salt. Highly reactive P species is generated by Mg reduction of PCl<sub>3</sub> at 250 °C in the

molten salt. Unlike organic solvents with high pressure upon heating, molten salts possess very low vapor pressure and better compatibility with inorganic reagents, thus possible for safe and efficient inorganic synthesis. The molten salt NaCl-KCl-AlCl<sub>3</sub> (20-16.5-63.5 mol%) has very low melting point ~90 °C<sup>[6]</sup>, which not only provide a liquid environment but also participate in the electron transport by the reversible conversion of Al<sup>3+</sup>/Al, thus enabling phosphorization at mild temperature.

PCl<sub>3</sub> is a widely used industrial chemical for manufacturing medicines, dyes, herbicides, plasticisers, oil additives and flame retardants.<sup>[7]</sup> The toxicity of PCl<sub>3</sub> is much lower than that of PH<sub>3</sub> or NaHPO<sub>2</sub>. More importantly, in our phosphorization method, only stoichiometric PCl<sub>3</sub> is required to complete the phosphorization process. The lower toxicity and high utilization of the phosphorous precursor makes this new method more benign for TMP nanostructure synthesis. Using this method, peapod CoP@C structure can be obtained by phosphorization of a Co@C nanostructure with same morphology, which exhibits excellent stability as a high-capacity anode material for lithium ion batteries.

The synthesis of the peapod-like CoP@C nanostructure is illustrated in Figure 1a. We first fabricate cobalt hydroxyl carbonate (CoOH(CO<sub>3</sub>)<sub>0.5</sub>·0.11H<sub>2</sub>O, CoHC, JCPDS 48-0084) nanowires by a hydrothermal method.<sup>[8]</sup> Then a polymeric glucose coating is deposited on the CoHC nanowires using glucose as the precursor by a hydrothermal method (CoHC@PG), which is subsequently converted to a peapod Co@C nanostructure (JCPDS 15-0806) by thermal treatment in Ar atmosphere. Owing to the hydrogen-bonding interaction between CoHC and glucose, the polymeric organic coating can be selectively formed on the surface of the CoHC nanowires through the dehydration of glucose. During the thermal treatment, the surface polymeric organics become a carbon shell and the CoHC nanowires are converted into Co nanoparticles encapsulated in the carbon shell, forming a peapod Co@C structure. The volume shrinkage during the CoHC-Co conversion leaves empty space between the encapsulated Co particles and the carbon shell. The structure and morphology conversion in the above processes are confirmed by XRD (Figure 1b) and SEM images (Figure 1c-e). The Co content in Co@C is 60 wt%.

To obtain peapod CoP@C structure, the peapod Co@C sample is mixed with PCl<sub>3</sub>, Mg powder in stoichiometric ratio and the low temperature molten salt NaCl-KCl-AlCl<sub>3</sub>. The mass ratio of the molten salt and PCl<sub>3</sub> is 10:1. The mixture is sealed in a Teflon-lined autoclave and heated at 250 °C for 24 h. The CoP@C sample is obtained by removing the salt with ethanol and deionized water. The XRD pattern shows that orthorhombic CoP phase (JCPDS 29-0497) is successfully obtained with complete conversion of Co. The energy-dispersive spectrum (EDS) further confirm the Co@P ratio is about 1:1 (Figure S1). The graphitized carbon can be inferred by the XRD peak at 26° and the Raman spectrum (Figure S2).<sup>[9]</sup> The SEM (Figure 1f)

[\*] Z.L. Liu, S.J. Yang, B.X. Sun, X. H. Chang, Dr. J. Zheng, Prof. Dr. X. G. Li, Beijing National Laboratory for Molecular Sciences (BNLMS), The State Key Laboratory of Rare Earth Materials Chemistry and Applications, College of Chemistry and Molecular Engineering, Peking University Beijing, 100871 (China) E-mail: jiezheng@pku.edu.cn, xgli@pku.edu.cn

X. H. Chang Academy for Advanced Interdisciplinary Studies, Peking University Beijing 100871 (China)

[†] These authors contributed equally

Supporting information for this article is given via a link at the end of the document.

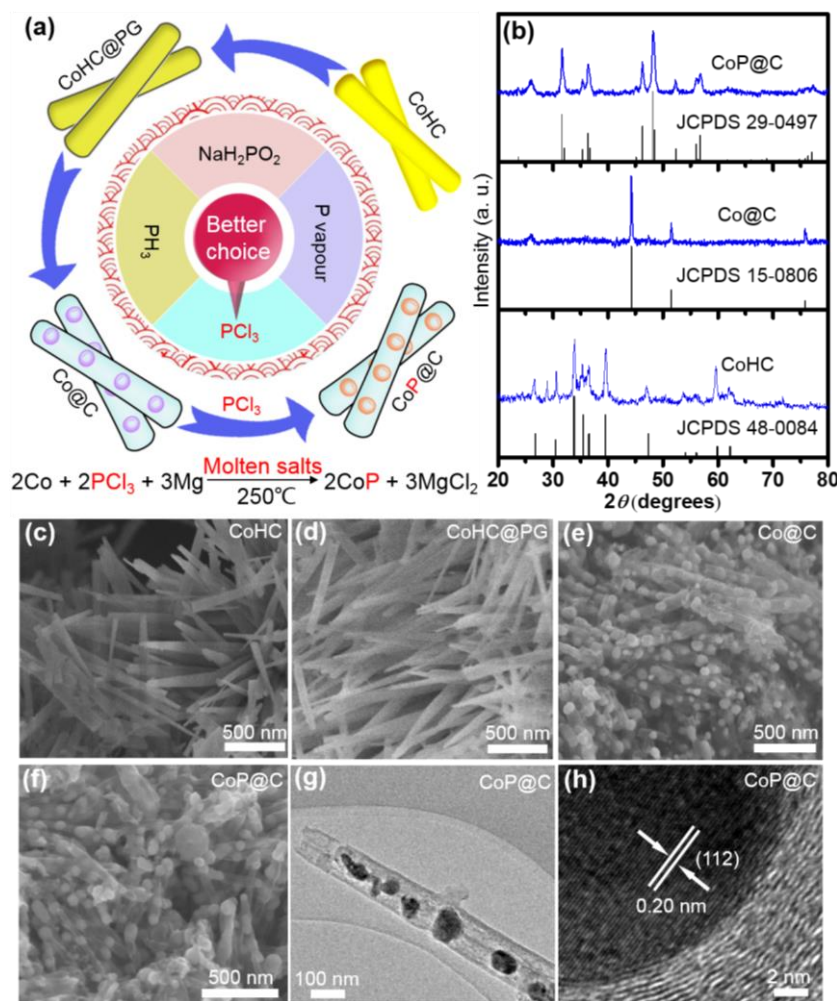


**Figure 1.** (a) The schematic illustration of synthesizing and fabricating of the peapod-like CoP@C nanostructures. (b) XRD patterns of the as-prepared CoOH(CO<sub>3</sub>)<sub>0.5</sub>·0.11H<sub>2</sub>O (CoHC), Co@C and CoP@C. (c-e) SEM images of CoHC (c), CoHC@PG (d) and peapod-like Co@C (e). (f-h) SEM (f), TEM (g) and HRTEM (h) images of peapod-like CoP@C.

and TEM (figure 1g) images of CoP@C clearly reflect the CoP nanoparticles with diameters less than 50 nm are uniformly wrapped by the 1D carbon nanotubular shells with well separated intervals. The well retained peapod morphology can be further confirmed by the large scale SEM image (Figure S3). In the high resolution TEM (HRTEM) image, the lattice fringes with interplanar distances of 0.2 nm can be resolved, which is corresponding to the (112) planes of CoP. In X-ray photoelectron spectroscopy (Figure S4), the peaks at 128.95, 131.5, 778.8 and 793.9 eV is ascribed to P 2p<sub>3/2</sub>, P 2p<sub>1/2</sub>, Co 2p<sub>3/2</sub> and Co 2p<sub>1/2</sub> of CoP phase respectively. Some oxidized peaks appear due to the surface oxidation of the CoP when exposed to air.<sup>[10]</sup> The carbon content in the CoP@C sample is about 30 wt%, as determined by elemental analysis.

Although the over-all reaction can be represented by Mg reduction of PCl<sub>3</sub> followed by phosphorization as shown in Figure 1a, some key links how the electrons from Mg leads to phosphorization of Co remain missing. To understand the phosphorization mechanism in molten NaCl-KCl-AlCl<sub>3</sub>, several control experiments are conducted.

First, the reaction is carried out without the Co@C sample. The water insoluble products after different reaction time is examined by XRD (Figure 2a). Metal aluminum is obtained in the first 24 h, while poorly crystallized red P appears only after 36 h accompanied with gradual consumption of Al. The above results indicate that AlCl<sub>3</sub> in the molten salt serves as the medium for electron transport through the reversible conversion of the Al<sup>3+</sup>/Al redox couple, which is also observed in previous studies by Lin et al.<sup>[11]</sup> As a result, the electrons from the Mg powder can be dispersed throughout the entire molten salt. A model of solvated electrons was proposed by some researchers.<sup>[12]</sup> As a result, the molten salt with Mg powder is a highly reductive medium. Phosphorization can readily occur even the Co surface is not in direct contact with the Mg powder.

When using commercial red P as the phosphorus source instead of PCl<sub>3</sub>, the CoP phase was unable to form, accompanied with large amount of residual red P (Figure S6). Unlike red P, PCl<sub>3</sub> can be homogeneously dispersed in the molten salt. Thus, the *in situ* generated P species by reduction of PCl<sub>3</sub> (designated by P\*) might be in the atomic scale and is much more reactive for phosphorization. It is also interesting to note that formation of the CoP phase requires much less time (< 24 h) compared to formation of the red P phase (~ 72 h), indicating that the Co nanoparticles also accelerate the reduction of PCl<sub>3</sub>. It was reported that there is strong coordination interaction between the Co surface and PCl<sub>3</sub>.<sup>[13]</sup> Thus, the PCl<sub>3</sub> molecules will be enriched on the Co surface and the P-Cl bonds will be weakened for easier reduction. The *in situ* generated P\*

species results in rapid phosphorization of the Co particles. The phosphorization mechanism is schematically illustrated in Figure 2b.

The peapod CoP@C sample is tested as the anode material for LIBs. Figure 3a displays the galvanostatic potential profiles 0.2 A g<sup>-1</sup>. The first discharge step shows three platforms around 1.2, 0.5 V and 0.01 V. The plateau at 1.2 V is associated with the electrolyte decomposition and formation of the solid electrolyte interface (SEI) layer. The plateau at 0.5 V is related to Li-ion insertion into the CoP forming a transition phase Li<sub>x</sub>CoP. The third plateau around 0.01 V is attributed to the Li<sub>x</sub>CoP being further reduced to Co and Li<sub>3</sub>P.<sup>[2, 14]</sup> The potential profiles is in good agreement with the cyclic voltammetry curve (Figure S7). It can be observed that the initial discharge capacity reaches about 1442 mAh g<sup>-1</sup>, with a high reversible charge capacity of 763 mAh g<sup>-1</sup>. The irreversible capacity in the first cycle is mainly attributed to the SEI formation.<sup>[15]</sup>

In order to further clarify the structural changes upon lithiation/delithiation, the CoP@C electrode at different lithiation stages (as indicated by the numbers in the potential profiles in Figure 3a) are analyzed by SEM and ex situ XRD. As shown in

Figure 3b, upon lithiation to 0.2 V, the CoP phase remains visible. An additional peak at 23° emerges, which is attributed to the transition phase  $\text{Li}_x\text{CoP}$ . The transition phase was proposed for CoP.<sup>[2, 16]</sup> and has been found during the lithiation of several transition metal phosphides ( $\text{Li}_x\text{CuP}$ ,  $\text{Li}_x\text{FeP}$ ).<sup>[17]</sup> In the fully lithiated electrode, only the graphite related peak at 26° is observed, indicating the formed  $\text{Li}_3\text{P}$  and Co phases are largely amorphous. As indicated by the SEM images (Figure 3d-f), the lithiation process is accompanied by a gradual disappearance of the CoP nanoparticles inside the peapod nanostructure, while the 1D morphology is well retained, which is in excellent agreement with the gradual phase transition suggested by XRD. The delithiation follows a perfect reverse process. The transition phase  $\text{Li}_x\text{CoP}$  first appears in the partially delithiated stage (IV) and the CoP phase is restored in the fully delithiated stage (V), albeit with poorer crystallinity. The nanoparticles inside the peapod structure is also well restored (Figure 3h). The highly reversible structure change of the peapod CoP@C structure during lithiation/delithiation is schematically illustrated in Figure 3c.

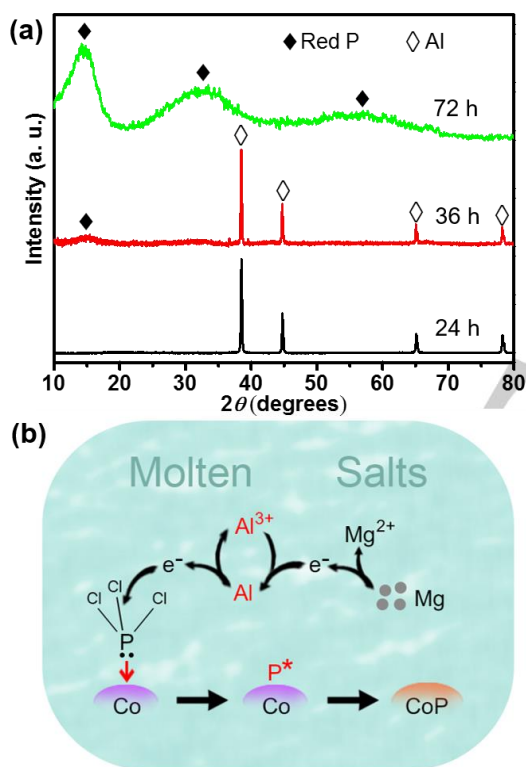


**Figure 2.** (a) XRD patterns of reaction products between Mg and  $\text{PCl}_3$  without Co@C in molten NaCl-KCl- $\text{AlCl}_3$  at 250 °C for different reaction time. (b) The schematic illustration of phosphorization mechanism in molten NaCl-KCl- $\text{AlCl}_3$ .

The stability of peapod-like CoP@C was evaluated by galvanostatic charge/discharge cycling at 0.2  $\text{A}\cdot\text{g}^{-1}$  (Figure 4a). The charge capacity remains about 720  $\text{mAh}\cdot\text{g}^{-1}$  after 50 cycles at 0.2  $\text{A}\cdot\text{g}^{-1}$ , corresponding to high capacity retention up to 94% compared to the first-cycle charge capacity. The specific capacity are based on the total mass of CoP@C. Figure 4b shows the capacities of the peapod CoP@C at different current density. The specific capacity is 770, 690, 560, 490, 420 and 340  $\text{mAh}\cdot\text{g}^{-1}$  at 0.1, 0.2, 0.5, 1.0, 2.0, and 5.0s  $\text{A}\cdot\text{g}^{-1}$ , respectively. When the current density is switched back to 0.1  $\text{A}\cdot\text{g}^{-1}$ , a high capacity of 650  $\text{mAh}\cdot\text{g}^{-1}$  can be rapidly restored. Remarkably,

the peapod CoP@C anode possesses excellent cycling stability at high current densities of 1.0  $\text{A}\cdot\text{g}^{-1}$ , delivering a stable capacity of 500  $\text{mAh}\cdot\text{g}^{-1}$  after 800 cycles (Figure 4c). As shown in Figure S8, the potential profiles of the 800<sup>th</sup> cycle are almost identical compared to the 20<sup>th</sup> cycle. The excellent cycling stability is further confirmed by electrochemical impedance spectroscopy (Figure S9). Some macroscopic parameters related to the interface charge transfer and  $\text{Li}^+$  diffusion can be obtained by fitting the Nyquist plot (shown in Table S1). There is almost no deterioration of the charge transfer and  $\text{Li}^+$  diffusion kinetics even after long cycles (seeing supporting information for detailed fitting process).

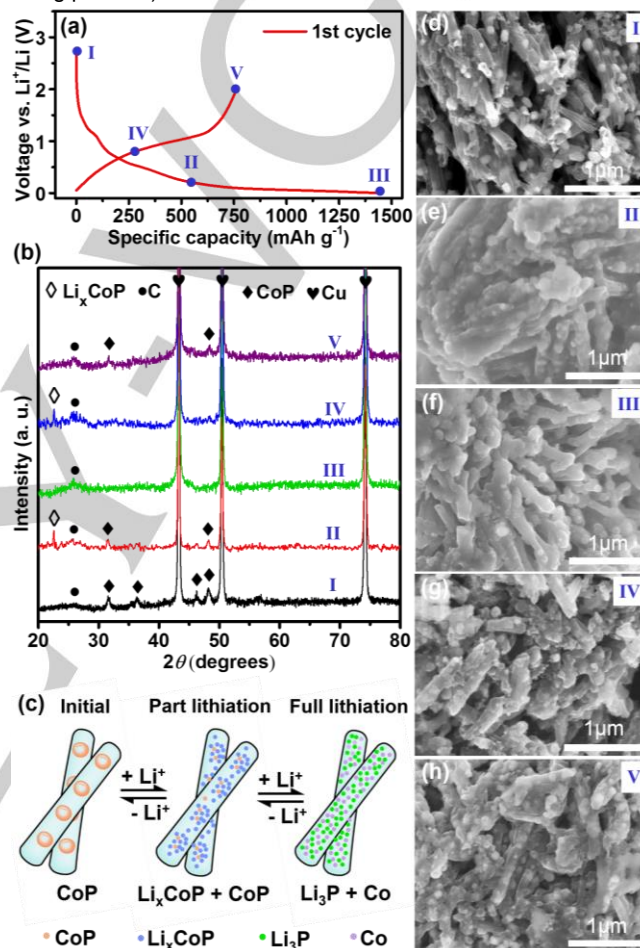


**Figure 3.** (a) The potential–capacity profile of the first cycle at 0.2  $\text{A}\cdot\text{g}^{-1}$ . (b) The XRD pattern of peapod CoP@C electrode at different stages as indicated by the numbers in (a). (c) The schematic illustration of reversible structure change of peapod CoP@C during lithiation/delithiation. (d–h) The SEM images of peapod-like CoP@C at different lithiation/delithiation states: (d) Initial electrode, (e) lithiation to 0.2 V, (f) lithiation to 0.005 V, (g) delithiation to 0.8 V, (h) delithiation to 2 V.

The long cycling life and excellent rate performance are mainly ascribed to the excellent structure stability of the CoP@C peapod nanostructure. As shown in Figure 3, the structure change during a charge/discharge cycle is highly reversible. Even after 800 cycles, the peapod structure and the encapsulated CoP particles can still be clearly observed (Figure S11). The unique 0D-in-1D structure offers sufficient space for the expansion of CoP during lithiation and a continuous conducting framework for electron transport as well as

accessible nanoporous channels for fast diffusion and transport of  $\text{Li}^+$ . The performance of the peapod  $\text{CoP@C}$  sample in this work, especially the rate performance and stabilities at large current density, is highly competitive compared to other transition metal phosphides.<sup>[2, 14, 18]</sup> A detailed comparison is shown in Table S2. In addition, the lithium storage performance of the  $\text{CoP@C}$  structure can be further improved by optimizing the  $\text{CoP}$  particle size and the thickness of the carbon layer.

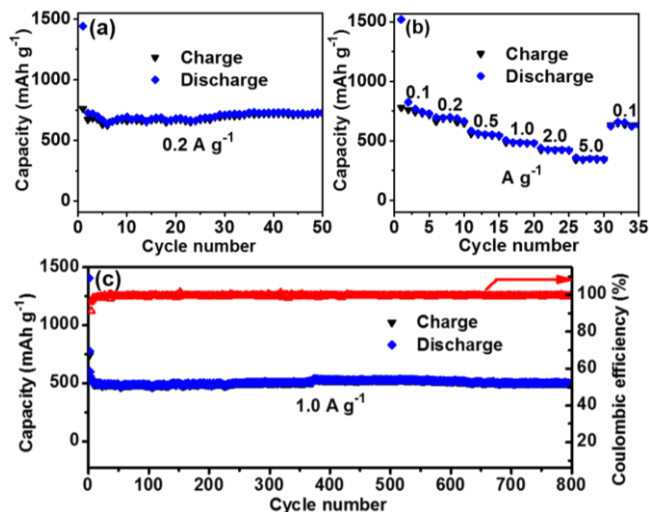


**Figure 4.** Lithium storage performance of peapod-like  $\text{CoP@C}$ . (a) Cycling performance at  $0.2 \text{ A g}^{-1}$ . (b) Rate performance at current densities ranging from  $0.1$  to  $5 \text{ A g}^{-1}$ . (c) Long cycling performance at  $1.0 \text{ A g}^{-1}$ . The first two cycles are tested at  $0.2 \text{ A g}^{-1}$  to activate the electrode.

The phosphorization method reported in this work is quite versatile. Other transition metals (such as Ni) and oxides can also be used as precursors to prepare the corresponding phosphides (Figure S12-13). Thus, the phosphorization method reported here brings vast opportunities in developing phosphide functional materials with controlled nanoscale morphology by combining with the well-established preparation methods for metals, oxides and metal/carbon nanocomposites.

In summary, we developed a mild phosphorization method based on reduction of  $\text{PCl}_3$  using Mg powder in low temperature molten salt ( $\text{NaCl-KCl-AlCl}_3$ ) to convert a peapod  $\text{Co@C}$  nanocomposite into  $\text{CoP@C}$  nanocomposite with the same morphology, which exhibits excellent lithium storage performances. Mechanism study suggests that the highly reactive  $\text{P}^*$  intermediate *in situ* formed by reduction of  $\text{PCl}_3$  leads to efficient phosphorization in mild conditions. This new method is advantageous for the lower toxicity and high utilization of the phosphorus precursor, which is very useful for the development of phosphide based functional nanostructures.

## Acknowledgements

The authors acknowledge the financial support from MOST of China (No. 2017YFB0405902) and National Science Foundation of China (NSFC, No. 21771006, U1607126, 51431001, 51771002 and 21621061).

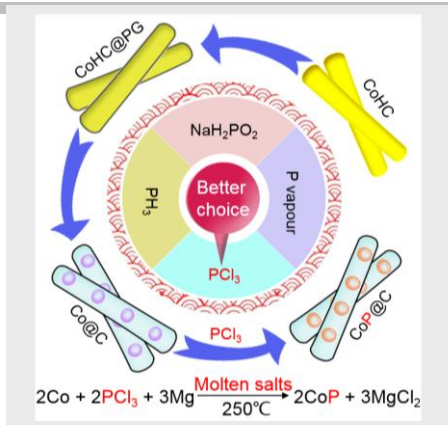
**Keywords:** Transition metal phosphides • phosphorization • low-temperature molten salt • synthesis design • batteries

- [1] a) H. Sun, X. Xu, Z. Yan, X. Chen, F. Cheng, P. S. Weiss, J. Chen, *Chem. Mater.* **2017**, *29*, 8539-8547; b) Y. Shi, B. Zhang, *Chem. Soc. Rev.* **2016**, *45*, 1529-1541; c) X. Li, W. Liu, M. Zhang, Y. Zhong, Z. Weng, Y. Mi, Y. Zhou, M. Li, J. J. Cha, Z. Tang, H. Jiang, X. Li, H. Wang, *Nano Lett.* **2017**, *17*, 2057-2063.
- [2] X. Xu, J. Liu, R. Hu, J. Liu, L. Ouyang, M. Zhu, *Chem. Eur. J.* **2017**, *23*, 5198-5204.
- [3] a) X. Wang, Y. V. Kolen'ko, X.-Q. Bao, K. Kovnir, L. Liu, *Angew. Chem., Int. Ed.* **2015**, *54*, 8188-8192; b) K. Zhang, M. Park, J. Zhang, G.-H. Lee, J. Shin, Y.-M. Kang, *Nano Res.* **2017**, *10*, 4337-4350.
- [4] a) H. Liang, A. N. Gandi, D. H. Anjum, X. Wang, U. Schwingenschlogl, H. N. Alshareef, *Nano Lett.* **2016**, *16*, 7718-7725; b) Y. Zhong, L. Yin, P. He, W. Liu, Z. Wu, H. Wang, *J. Am. Chem. Soc.* **2018**, *140*, 1455-1459.
- [5] a) P. He, X.-Y. Yu, X. W. Lou, *Angew. Chem., Int. Ed.* **2017**, *56*, 3897-3900; b) X. Ge, Z. Li, L. Yin, *Nano Energy* **2017**, *32*, 117-124.
- [6] H. Zhang, K. Dasbiswas, N. B. Ludwig, G. Han, B. Lee, S. Vaikuntanathan, D. V. Talapin, *Nature* **2017**, *542*, 328-331.
- [7] a) J. Kobayashi, A. Ishikawa, Y. Ishino, T. Ono, T. Ito, M. Mihara, *JP2007223934A*, **2007**; b) M. Honjo, R. Marumoto, *US3346562*, **1967**; c) G. F. Karkozova, S. G. Lyubetskii, L. I. Zyuzina, A. L. Gol'denberg, A. G. Sirota, *Plast. Massy* **1970**, 33-36.
- [8] J. Jiang, J. P. Liu, X. T. Huang, Y. Y. Li, R. M. Ding, X. X. Ji, Y. Y. Hu, Q. B. Chi, Z. H. Zhu, *Cryst. Growth Des.* **2010**, *10*, 70-75.
- [9] H. Ye, C.-Y. Wang, T.-T. Zuo, P.-F. Wang, Y.-X. Yin, Z.-J. Zheng, P. Wang, J. Cheng, F.-F. Cao, Y.-G. Guo, *Nano Energy* **2018**, *48*, 369-376.
- [10] B. Wang, Q. Ru, Q. Guo, X. Chen, Z. Wang, X. Hou, S. Hu, *Eur. J. Inorg. Chem.* **2017**, *2017*, 3729-3735.
- [11] N. Lin, Y. Han, L. Wang, J. Zhou, J. Zhou, Y. Zhu, Y. Qian, *Angew. Chem., Int. Ed.* **2015**, *54*, 3822-3825.
- [12] X. Liu, C. Giordano, M. Antonietti, *J. Mater. Chem.* **2012**, *22*, 5454-5459.
- [13] N. Takagi, A. Krapp, G. Frenking, *Z. Anorg. Allg. Chem.* **2011**, *637*, 1728-1735.
- [14] J. Jiang, C. Wang, W. Li, Q. Yang, *J. Mater. Chem. A* **2015**, *3*, 23345-23351.
- [15] A. Casimir, H. Zhang, O. Ogoke, J. C. Amine, J. Lu, G. Wu, *Nano Energy* **2016**, *27*, 359-376.
- [16] R. Khatib, A. L. Dalverny, M. Saubanere, M. Gaberscek, M. L. Doublet, *J. Phys. Chem. C* **2013**, *117*, 837-849.
- [17] a) S. Boyanov, D. Zitoun, M. Menetrier, J. C. Jumas, M. Womes, L. Monconduit, *J. Phys. Chem. C* **2009**, *113*, 21441-21452; b) X. He, R. Wang, M. C. Stan, E. Paillard, J. Wang, H. Frielinghaus, J. Li, *Adv. Mater. Interfaces* **2017**, *4*, 1601047-1601055.
- [18] a) K. Zhu, J. Liu, S. Li, L. Liu, L. Yang, S. Liu, H. Wang, T. Xie, *Adv. Mater. Interfaces* **2017**, *4*, 1700377-1700384; b) D. Yang, J. Zhu, X. Rui, H. Tan, R. Cai, H. E. Hoster, D. Y. W. Yu, H. H. Hng, Q. Yan, *ACS Appl. Mater. Interfaces* **2013**, *5*, 1093-1099; c) H.-T. Kwon, J.-H. Kim, K.-J. Jeon, C.-M. Park, *RSC Advances* **2014**, *4*, 43227-43234; d) H. Guo, C. Chen, K. Chen, H. Cai, X. Chang, S. Liu, W. Li, Y. Wang, C. Wang, *J. Mater. Chem. A* **2017**, *5*, 22316-22324; e) Y. Lu, J.-P. Tu, Q.-Q. Xiong, J.-Y. Xiang, Y.-J. Mai, J. Zhang, Y.-Q. Qiao, X.-L. Wang, C.-D. Gu, S. X. Mao, *Adv. Funct. Mater.* **2012**, *22*, 3927-3935; f) Y. Zhang, H. Zhang, Y. Feng, L. Liu, Y. Wang, *ACS Appl. Mater. Interfaces* **2015**, *7*, 26684-26690; g) X. Wang, K. Chen, G. Wang, X. Liu, H. Wang, *ACS Nano* **2017**, *11*, 11602-11616.

## Entry for the Table of Contents

## COMMUNICATION

A significant breakthrough for the development of phosphide based functional materials: mild phosphorization with low-toxic phosphorus source in low-temperature molten salt for high-efficiency synthesis of peapod-like CoP@C with superior lithium storage performance.



Zhiliang Liu, Sungjin Yang, Bingxue Sun, Xinghua Chang, Jie Zheng\*, Xingguo Li\*

Page No. – Page No.

**Peapod-like CoP@C nanostructure from phosphorization in low-temperature molten salt for high-performance lithium ion batteries**